AACVD Grown WO_3 Nanoneedles Decorated with Ag/Ag_2O Nanoparticles for Oxygen Measurement in a Humid Environment

Wangi P. Sari[1*], Chris Blackman[2], Yiyun Zhu[2], James Covington[1]

Abstract—**A sensitive material consisting of silver/silver oxide decorated WO_3 was successfully grown in two steps via aerosol-assisted chemical vapour deposition (AACVD). Morphological, structural, and composition analysis revealed our method is effective for growing WO_3 nanoneedles decorated with silver/silver oxide nanoparticles at relatively low temperature (≤ 375°C) onto sensor arrays printed on alumina substrate. The sensors were tested for oxygen under humid environment (relative humidity ~85%) with the concentration ranging between 0% and 20%. Gas sensing results showed good response to oxygen with optimum temperature was observed at 400°C for undecorated WO_3 and at 350°C for silver/silver oxide decorated WO_3. The addition of silver/silver oxide was found to improve the sensor response by almost 300%, making the sensor a potential alternative to replace existing Pb-based oxygen sensor.**

Index Terms—Chemical sensor, heterojunction, oxygen detection, silver oxide, thin film sensor, tungsten oxide.

I. Introduction

Oxygen sensors are widely used for applications such as environmental monitoring, food and beverages, medical and pharmaceutical, and waste management industries. Currently, the market is dominated by electrochemical-based sensors that rely on the oxidation of lead in the anode. The sensors have been highly successful with no change for over 20 years. However, "Restriction of Hazardous Substances Directive" (RoHS) also known as Directive 2002/95/EC, prohibits use of lead in almost all electronic products. Gas sensors are exempt at the moment, but the ban will be applied to gas sensor market in the near future. Pb-free alternative electrochemical gas sensors for oxygen detection have been developed using zinc, iron or aluminium, and have made it to gas sensor market, but their use is still limited due to life-span and sensitivity issues. Moreover, these oxygen sensors are quite bulky in size, making it harder to integrate the sensors with micro-electronics. Other alternatives using optical methods are also available, either based on light absorbance or photo-quenching[1-3]. These work well but they require emitters and complex electronics to get a reading, thus again making the sensor quite bulky and more expensive. Another alternative for a lead-free oxygen sensor are the solid-state based sensors used heavily in the automotive industry. These sensors have proven reliability for measuring the air to fuel ratio for engine combustion system. However, they require high operating temperature in excess of 600°C, which make them unsuitable as a direct replacement for many Pb-based sensor applications. Therefore, there is a need for developing a new generation of compact, cost-effective, and reliable sensors to facilitate oxygen detection at lower temperatures.

MOX based sensors are one of the most commercially successful gas sensing technologies with market share exceeding 15% [4]. They detect gases by measuring resistive changes that occur due to a chemical reaction between a target gas and the sensing material. The technology offers advantages including simple measurement, low-cost manufacturing cost, and the ability to operate in harsh or high temperature environment. Furthermore, the technology enables easy integration with smart electronic devices associated with the internet of things (IoT).

Several metal oxide semiconductors such as SnO_2 [5], TiO_2 [6, 7], CeO_2 [8], In_2O_3 [9, 10], Ga_2O_3 [11] and ZnO [12, 13], have been explored as potential oxygen sensors. Ogita et al. reported Ga_2O_3 thin films for oxygen detection at high temperature over 600°C [11]. Chabooouni and coworkers studied the characteristics of oxygen detection using zinc oxide [12]. The films were operated at room temperature but the response was not reproducible (drifts were observed). Neri et al. were able to obtain reproducible response using functionalised indium oxide with optimum operating temperature at 200°C [14]. Hu et al. reported good response for detecting oxygen at lower temperature down to 40°C using nano-structured $SrTiO_3$ [15]. However, none of the papers previously cited investigated the effect of the ambient humidity on sensor performance, even though it is well known that humidity is a major drawback experienced in metal oxide sensors, reducing the sensors response [16, 17].

Previous work on MOX sensors (though not specifically for oxygen detection) have shown that by adding catalyst nanoparticles onto the metal oxide sensing material, the sensitivity and selectivity toward a targeted gas can be

This work was supported by Lembaga Pengelola Dana Pendidikan (LPDP), Ministry of Finance, Republic of Indonesia.

Wangi P. Sari is with the School of Engineering, University of Warwick, Coventry, CV4 7AL UK (email: w.p.sari@warwick.ac.uk).

Chris Blackman is with Dept of Chemistry, University College London, London, WC1E 6BT UK (email: c.blackman@ucl.ac.uk).

Yiyun Zhu is with Dept of Chemistry, University College London, London, WC1E 6BT UK (email: yiyun.zhu.14@ucl.ac.uk).

James Covington is with the School of Engineering, University of Warwick, Coventry, CV4 7AL UK (email: j.a.covington@warwick.ac.uk).

.

significantly improved [18-25]. In this work, we have fabricated functionalised and non-functionalised thin films by aerosol-assisted chemical vapour deposition (AACVD) method and investigated the sensor performance for oxygen detection in a humid environment as a potential replacement for Pb-based electrochemical sensors.

II. Experimental Section

A. Synthesis of Sensing Material

Tungsten oxide films were deposited on alumina gas sensor substrates by AACVD. The size of each individual substrate was 2 x 2 mm with a thickness of 250 µm. Gold interdigitated electrodes were printed on one side of the substrate and platinum heater on the other side. Before being placed inside the reactor, the substrates were cleaned with isopropanol and acetone and then left to dry in air. The precursor $W(CO)_6$ (0.060 g) (≥97%, Sigma Aldrich) was dissolved in a 2:1 mixture of acetone (≥99.6%, Sigma Aldrich) and methanol (≥99.6%, Sigma Aldrich) to a total of 15 ml. Aerosol was generated from the precursor solution using an ultrasonic humidifier (Johnson Matthey Liquifog operating at 2 MHz) and then transported to the reactor using nitrogen (99.99%, BOC) as the carrier gas flowing at 300 sccm. The precursor solution was transported at 375°C with the deposition time (time required to transport all the solution) between 30 and 40 minutes. Subsequently, the reactor was cooled down to room temperature. The samples were subjected to annealing in an oven at 500°C for 2 hours in air at 10°C/min before being cooled down to room temperature. The conditions were chosen as such to promote the morphology of WO_3 as previously reported [26].

Ag/Ag_2O NP-decorated WO_3 films were prepared via a two-step AACVD method. In the first stage, pure WO_3 films were deposited followed by annealing at 500°C for 2 hr. In the subsequent step, silver was incorporated to the film by dissolving precursor $AgNO_3$ (0.090 g) (≥99.0%, Scientific Laboratory Supplies) in 10 ml acetone and 5 ml methanol and then generating the aerosol from the precursor solution. The aerosol was deposited at 250°C via a nitrogen carrier at 300 sccm.

B. Material Analysis

XRD pattern of samples grown on alumina and glass substrates were collected using Bruker D8 Discover LynxEye thin-film PXRD. The elemental composition was performed by Thermo Scientific K-alpha X-ray photoelectron spectrometer. The morphology of the sensing materials was examined using a JEOL JSM-6301 Field Emission Scanning Electron Microscope. JEOL 2100 high resolution TEM was performed by removing the film from the substrate by sonification.

C. Oxygen Sensing Tests

Gas sensing tests were carried out using a dedicated gas handling apparatus previously constructed at the School of Engineering, University of Warwick. The gas rig can supply a predefined concentration of oxygen by diluting 99.999% nitrogen (Lehman Instrument, France) with zero air (20% O_2). The dilution is obtained by varying the flow rate of each gas using MFC (UFC 1100, Brooks) controlled by computer programme written in LabVIEW (National Instrument 2016). Humid environment was achieved by passing the gas mixture to a water bubbler before entering the sensor chamber and measurement was monitored and logged with a humidity data logger (Lascar Electronic).

The resistance changes of the different sensors while exposed to different oxygen concentrations were monitored and logged by a sensor management system AS-330 (Atmospheric Sensor Ltd, UK). Using the device, different ranges of operating temperature, test period, and operating sequence can be tested. The sensors were exposed to a different test environment in a 30-minute cycle. Oxygen concentration ranged between 0% and 20%. The chamber was subsequently purged with N_2 for 30 minutes to enable sensor recovery to the baseline value and stabilise before a new measurement was taken. The sensor response was defined as being equal to R_g/R_a where R_g is the sensor baseline in the reference as N_2 and R_a is the sensor resistance is the resistance of targeted gas O_2 in the reference gas. The response and recovery time of the sensors were defined as the corresponding time to a 90% change in the electrical resistance of the samples.

III. Results and Discussion

A. Material Characterisation

The XRD patterns from annealed samples of undecorated WO_3 and Ag/Ag_2O-WO_3 (Fig. 1) showed the presence of peaks associated with monoclinic phase of tungsten oxide with strong orientation in the (002) direction (γ-WO3 structure, P2*1*/*n*, *a* = 7.30084(7), *b* = 7.53889(7), *c* = 7.68962(7) Å, β = 90.892(1)°), as previously observed [27-29]. No peaks for silver or silver oxide were observed in decorated samples, possibly due to the small size and/or the relatively low amount present. Comparison of undecorated and decorated samples revealed no shifts in WO_3 peak positions, which demonstrate that the monoclinic crystal structure of WO_3 was not changed during the addition of Ag.

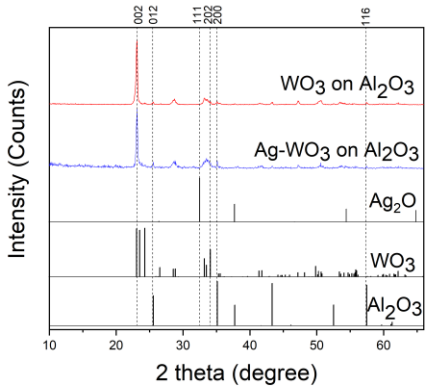

Fig. 1. XRD patterns of annealed samples of undecorated and decorated WO_3 deposited on alumina substrates.

This article has been accepted for publication in a future issue of this journal, but has not been fully edited. Content may change prior to final publication. Citation information: DOI 10.1109/JSEN.2018.2878051, IEEE Sensors Journal

XPS was carried out to obtain more detailed information on the elemental composition. Analysis of W 4f core-level spectrum from pure WO_3 sample showed identical result with Ag/Ag_2O-WO_3 sample. As illustrated in Fig. 2a, the W 4f spectrum showed the presence of two intense peaks centred at 35.5 and 37.6 eV associated with the W $4f_{7/2}$ and W $4f_{5/2}$ doublets respectively. These binding energies are similar with reference values for stoichiometric WO_3 with the oxidation state W^{6+} [30]. Fig. 2b displays the XPS of Ag 3d core level spectrum where two intense peaks can be observed at 367.7 and 373.6 eV associated with the Ag $3d_{5/2}$ and Ag $3d_{3/2}$ respectively. The highest intensity peak (Ag $3d_{5/2}$) corresponds to Ag_2O and the absence of a loss peak confirms the assignment [31].

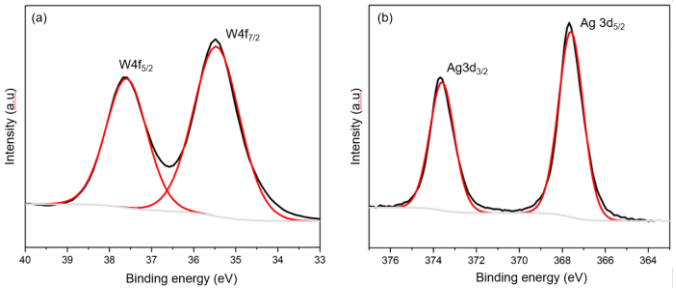

Fig. 2. XPS spectrum of the silver decorated WO_3 nanoneedles after annealing: (a) W 4f and (b) Ag 3d.

SEM imaging of the annealed films (Fig. 3) showed a high density of non-aligned nanoneedles with uniform dimension, which were unchanged between WO_3 and Ag/Ag_2O-decorated WO_3 films. Measurement of the NNs showed length at about 1300 nm with diameters varied between 100 and 200 nm. The film displayed a quite porous body structure, which is desired in gas sensing application as it can facilitate gas adsorption.

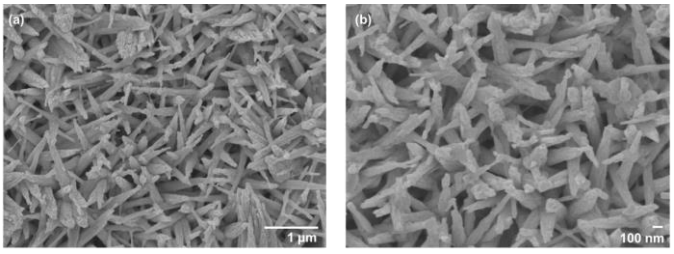

Fig. 3. Film morphologies observed by SEM images at: (a) low and (b) high magnification. Non-functionalised (WO_3) and functionalised NN films (Ag-WO_3) show the same morphology.

Details on the morphological features of Ag/Ag_2O-WO_3 were further examined by HR-TEM. In this work, the results obtained from the pure WO_3 are not shown as they were similar to the ones we reported previously [19]. HR-TEM images in Fig. 4 displays the presence of well-dispersed nanoparticles along the surface of WO_3 nanoneedles, similar with the ones seen for gold and palladium functionalized WO_3 NNs [28, 32]. Cubic Ag_2O with (111) crystal planes (d=0.274 nm) can be confirmed from the fringe image (Fig 4b). Here, we also observed Ag metal (d=0.238 nm) which is present alongside Ag_2O. The combined XPS and TEM analysis suggest the particles observed are an Ag/Ag_2O 'core-shell', e.g. an Ag core where the air-exposed faces are oxidised to Ag_2O, although the absence of satellite peaks for Ag metal in the XPS analysis suggests the shell must be thicker than ~ 2 nm.

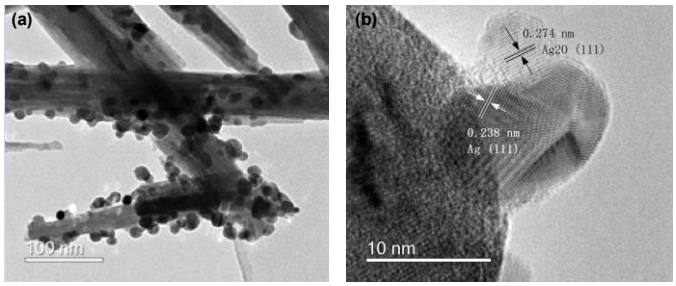

Fig. 4. HR-TEM images of Ag-WO_3 samples.

B. *Gas Response*

Gas-sensing tests were carried out to different oxygen concentration in a humid environment. Undecorated and silver/silver oxide decorated WO_3 NNs sensors were tested at temperatures ranging between 150 and 400°C in 50°C interval to examine the effect of temperature on sensor performances (Fig 5). Very little resistance change was observed for WO_3 and Ag/Ag_2O-WO_3 NNs at temperatures lower than 200°C, which lead to almost no response to changes in oxygen concentration. As the temperature increased, WO_3 exhibited higher response with the maximum observed at 400°C (R_g/R_a = 8). For the Ag/Ag_2O-decorated WO_3 sensor, the response reached maximum response at 350°C (R_g/R_a = 23). Thus, 400°C and 350°C are the optimal operating temperature for undecorated and decorated WO_3 NN sensors.

Decoration of silver/silver oxide nanoparticles promoted a higher response in addition to lowering the operating temperature. For example, the response of pure WO_3 NNs at 250°C was equal to R_g/R_a=4 whereas Ag/Ag_2O-WO_3 exhibited response at R_g/R_a=7.8. At their optimum temperature, the response was increased by nearly 4 times with the operating temperature being lowered by 50°C. The amount of silver present also influenced sensor response as a higher response is reported here in comparison to our previous work with lower Ag content [33].

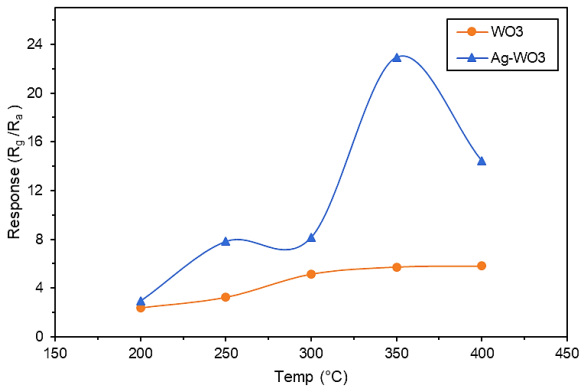

Fig. 5. Sensor responses to 20% O_2 as a function of the operating temperature at 85% RH.

This article has been accepted for publication in a future issue of this journal, but has not been fully edited. Content may change prior to final publication. Citation information: DOI 10.1109/JSEN.2018.2878051, IEEE Sensors Journal

Fig. 6 displays the change in the resistance of undecorated and Ag/Ag_2O-decorated WO_3 sensors toward O_2 concentration ranging from 0 to 20%. As expected from an n-type semiconductor behaviour, the sensor resistance increased upon exposure to oxidising gases, such as O_2 and reduced in presence of N_2. Decorated sensors showed a lower resistance in the range of 10^3-10^4 Ω in comparison to WO_3 film at 10^5-10^6 Ω. Here, we can observe small changes/drifts in the baseline as well in the as response to 20% O_2 from undecorated and decorated sample. Replicate measurements revealed that baseline of undecorated sensor varied from 44 to 54 kΩ whereas the response to 20% O_2 varied from 235 to 260 kΩ. As metal oxide based sensors rely on a chemical reaction in detecting a target gas, these variations are inevitable. Our calculations showed that the values were deviated by 10% for the baseline and 5% for the response. As for Ag/Ag_2O-WO_3 sensor, the variations were found to be slightly higher, i.e. 2 ± 0.5 kΩ (25%) for the baseline and 24 ± 1.5 kΩ (6.25%). Nonetheless, we found these values are comparable to resistance variations found in commercial sensors, indicating good performance from our sensors.

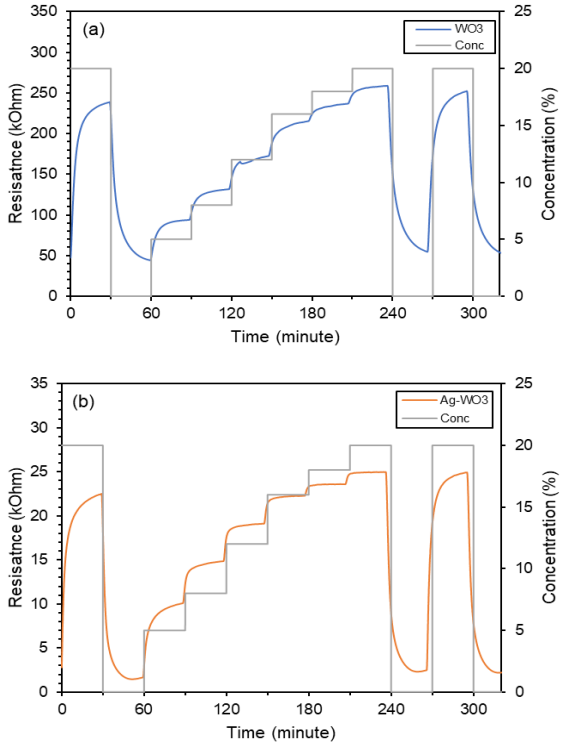

Fig. 6. Sensor resistance changes of (a) WO_3 and (b) Ag-WO_3 film to various O_2 concentration at 85% RH.

At 20% O_2, the response and recovery times were calculated for undecorated and decorated WO_3 nanoneedles. The results indicate that increasing the operating temperature generally improved the rate of response and recovery, as illustrated in Fig. 7. Functionalised samples recorded a response time in 9.2 minutes (350°C), faster than response time of bare WO_3 samples at 11.5 minutes (400°C). A complete recovery of the baseline was observed at 9 and at 13.7 minutes for Ag/Ag_2O-WO_3 and WO_3 samples respectively. Overall, decorated samples showed a faster response and recovery time in all temperature ranges. When these results are compared with the ones reported in the literature for metal oxide based sensors, the rate of response of our sensors are quite fast considering the relatively low operating temperature. These rates are faster than previously reported Pt-doped In_2O_3 sensor operated at room temperature with response and recovery time at 18 and 35 minutes respectively [10]. Faster response rate was reported for Ga_2O_3 based films at 14 seconds, but the sensors were operated at a high temperature 1000°C [11]. Similarly, response time was observed at 9 seconds for TiO_2 based films operated at 800°C [7]. A study on palladium decorated WO_3 to detect H_2 reported a very fast response (i.e. 2 minutes) at 390°C but the recovery rate was much slower at 18.3 minutes [32].

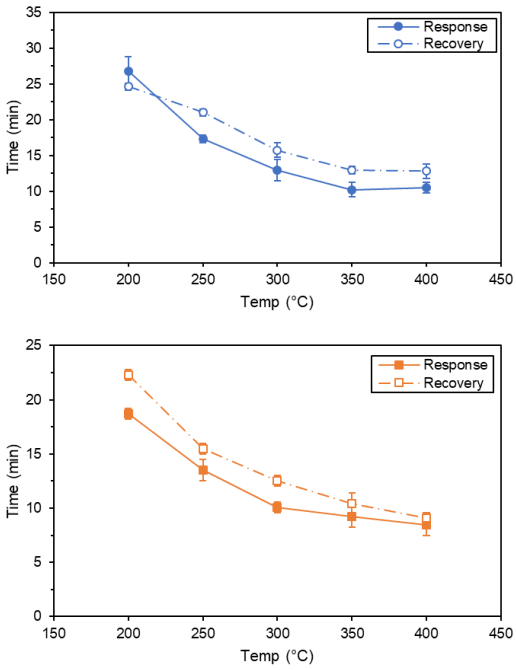

Fig. 7. Response and recovery time of: (a) WO_3 and (b) Ag-WO_3 sensors at various operating temperature.

The corresponding gas-sensing responses are plotted as a function of oxygen concentration as shown in Fig. 8. The results indicate oxygen concentration changing linearly for undecorated films whereas decorated films follow a traditional power law relationship (alpha value = 0.76), which is commonly found in metal oxide-based sensors. Power law relationship expresses concentration dependency at a certain range. In this case, Ag/Ag_2O-WO_3 films show $pO_2^{0.76}$ dependencies toward oxygen concentration in range 5 – 20%. The alpha value is critical in determining whether good discrimination of oxygen can be obtained. Generally, values between 0.5 and 1.0 are good with values closer to 1.0 showing better oxygen differentiation. Therefore, it can be concluded that our sensors exhibit good differentiation toward oxygen at said range.

Tungsten oxide based sensors have been shown to respond

to a range of different volatile organic compounds [34-37] and interference gases such as NH_3, CO, and NO_2 [38-41]. In order to fully utilise the sensors for oxygen detection, strategies are required to minimize the impact of cross-sensitivity. One of the common approach used in commercial sensors is to use passive filters, packaged with the sensors, to diminish interference and make the sensor more targeted to a particular compound. Our future work will focus on investigating the selectivity of the sensors to other gases and working to resolve the issues before making a further judgement on the full potential of the decorated WO_3 films as oxygen sensors.

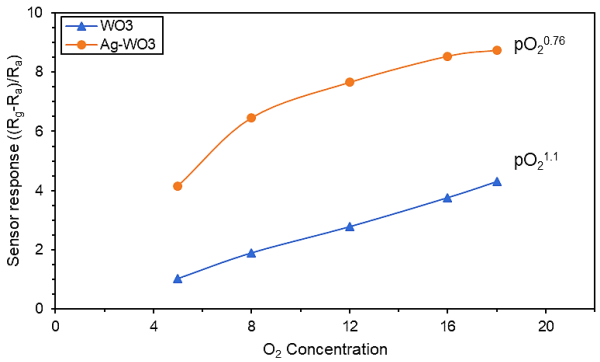

Fig. 8. Sensor responses toward various oxygen concentration.

C. *Sensing Mechanism*

The fabricated sensor showed no response at temperatures ≤150°C. Although sensors started to respond at 200°C, with the best response noted at 400°C for bare WO_3 films and 350°C for decorated WO_3 films. At lower temperatures, it is likely that not enough energy is present to facilitate adsorption/desorption process of oxygen species during gas exposure. Silver decoration in the thin films have improved sensor performance and reduced the optimum operating temperature. The role of catalyst in metal oxide to detect targeted gases has been proposed by two sensitisation mechanisms, i.e. chemical and electronic sensitisation [42]. In chemical sensitisation, silver oxide nanoparticles could facilitate the chemical reactions and increase chemical rate between oxygen molecules and tungsten oxide surface via spill-over mechanism [42, 43]. On the other hand, electronic sensitisation occurs through a direct electron interaction between the additives and metal oxide surface.

For silver oxide catalyst, electronic sensitisation is more likely to occur under reduction to metal with an inflammable gas [42]. Upon contact the Ag_2O shell will exchange electrons with WO_3, with the direction of exchange expected be toward WO_3 (data found in literature showing the conduction band of Ag_2O at -1.3 eV [44, 45] whilst WO_3 is at 0.4 eV [46]). The potential difference provides a considerable driving force for the electrons from Ag_2O to populate the conduction band of WO_3. For an n-type semiconductor, this would increase the carrier concentration and hence reduce the baseline resistance of the sensors, which we observe experimentally. However, this electron exchange would not explain an enhanced sensitivity toward O_2. It is possible that changes in oxygen partial pressure would change electron density at the Ag_2O shell and this is reflected by a measured change in resistance in the WO_3, but we have no evidence to be able to assert this. On the other, we also cannot rule out spill-over taking place whereby Ag_2O could act to spill-over oxygen, increasing the population of O_2 on the surface. If the Ag_2O enrich WO_3 with oxygen species, this could explain a higher sensitivity towards oxygen, however this might be expected to increase the baseline resistance in ambient air, although it could be difficult to disentangle the electronic effect on baseline resistance from any attributable to spill-over.

IV. Conclusion

Tungsten oxide nanoneedles decorated with silver/silver oxide nanoparticles were successfully grown by a two-step AACVD method. The gas-sensing results revealed that the silver oxide decoration of significantly improved the sensor performance by 400% and lower the optimum temperature from 400°C to 350°C. The functionalised sensors showed a good oxygen differentiation in humid environment, following a power law relationship with alpha value 0.76. Further investigation on sensor selectivity and cross-sensitivity to other gases will be carried out in the future, as well as looking at the effects of varying humidity levels in order to obtain a better assessment on tungsten oxide full potential as oxygen sensors.

References

[1] A. Hiroaki, K. Tooru, and K. Shuji, "Fluorescence oxygen sensor using photo quenching with oxygen molecule," in *SICE Annual Conference 2007*, 2007, pp. 1762-1765.

[2] N. Shehata, K. Meehan, I. Ashry, I. Kandas, and Y. Xu, "Lanthanide-doped ceria nanoparticles as fluorescence-quenching probes for dissolved oxygen," *Sensors and Actuators B: Chemical*, vol. 183, pp. 179-186, 2013/07/05/ 2013.

[3] R. C. Evans, P. Douglas, J. A. G. Williams, and D. L. Rochester, "A Novel Luminescence-Based Colorimetric Oxygen Sensor with a "Traffic Light" Response," *Journal of Fluorescence*, vol. 16, no. 2, pp. 201-206, 2006/03/01 2006.

[4] I. Grand View Research, "Gas Sensor Market Size, Share & Trends Analysis Report By Product, By Technology, By End Use (Medical, Petrochemical, Automotive, Industrial), By Region, And Segment Forecasts, 2018 - 2025," 978-1-68038-083-5, 2018, Available: https://www.grandviewresearch.com/industry-analysis/gas-sensors-market, Accessed on: 20 June 2018.

[5] J. Atkinson , A. Cranny, and C. Simonis de Cloke, "A low-cost oxygen sensor fabricated as a screen-printed semiconductor device suitable for unheated operation at ambient temperature," *Sensors and Actuators B: Chemical*, vol. 47, pp. 171-180, 1998.

[6] R. K. Sharma, M. C. Bhatnagar, and A. L. Sharma, "Mechanism in Nb doped titania oxygen gas sensor," *Sensors and Actuators B: Chemical*, vol. 4, pp. 194-201, 1998.

[7] R. K. Sharma, M. C. Bhatnagar, and G. L. Sharma, "Mechanism of highly sensitive and fast response Cr doped TiO2 oxygen gas sensor," *Sensors and Actuators B: Chemical*, vol. 45, no. 3, pp. 209-215, 1997/12/15/ 1997.

[8] N. Izu, W. Shin, N. Murayama, and S. Kanzaki, "Resistive oxygen gas sensors based on CeO2 fine powder," *Sensors and Actuators B*, vol. 87, pp. 95-98, 2002.

[9] D. Selvakumar, N. Dharmaraj, N. S. Kumar, and V. C. Padaki, "Oxygen Sensing Properties of Platinum Doped Indium Oxide Nanoparticles Prepared by Hydrothermal Method," *Synthesis and Reactivity in Inorganic, Metal-Organic, and Nano-Metal Chemistry*, vol. 45, no. 5, pp. 753-758, 2014.

[10] G. Neri *et al.*, "A highly sensitive oxygen sensor operating at room temperature based on platinum-doped In2O3 nanocrystals," *Chem Commun (Camb)*, no. 48, pp. 6032-4, Dec 28 2005.

[11] C. Baban, Y. Toyoda, and M. Ogita, "Oxygen sensing at high temperatures using Ga2O3 films," *Thin Solid Films*, vol. 484, no. 1–2, pp. 369-373, 7/22/ 2005.

[12] F. Chaabouni, M. Abaab, and B. Rezig, "Metrological characteristics of ZNO oxygen sensor at room temperature," *Sensors and Actuators B: Chemical*, vol. 100, no. 1-2, pp. 200-204, 2004.

[13] H. Minaee, S. H. Mousavi, H. Haratizadeh, and P. W. de Oliveira, "Oxygen sensing properties of zinc oxide nanowires, nanorods, and nanoflowers: The effect of morphology and temperature," *Thin Solid Films*, vol. 545, pp. 8-12, 2013/10/31/ 2013.

[14] G. Neri, A. Bonavita, G. Micali, G. Rizzo, N. Pinna, and M. Niederberger, "In2O3 and Pt-In2O3 nanopowders for low temperature oxygen sensors," *Sensors and Actuators B: Chemical*, vol. 127, no. 2, pp. 455-462, 2007.

[15] Y. Hu, O. K. Tan, W. Cao, and W. Zhu, "A low temperature nano-structured SrTiO3 thick film oxygen gas sensor," *Ceramics International*, vol. 30, no. 7, pp. 1819-1822, // 2004.

[16] G. Korotcenkov, I. Blinov, V. Brinzari, and J. R. Stetter, "Effect of air humidity on gas response of SnO2 thin film ozone sensors," *Sensors and Actuators B: Chemical*, vol. 122, no. 2, pp. 519-526, 2007/03/26/ 2007.

[17] Z. Bai, C. Xie, M. Hu, S. Zhang, and D. Zeng, "Effect of humidity on the gas sensing property of the tetrapod-shaped ZnO nanopowder sensor," *Materials Science and Engineering: B*, vol. 149, no. 1, pp. 12-17, 2008/03/15/ 2008.

[18] F. E. Annanouch *et al.*, "Aerosol-Assisted CVD-Grown WO3 Nanoneedles Decorated with Copper Oxide Nanoparticles for the Selective and Humidity-Resilient Detection of H2S," *ACS Applied Materials & Interfaces*, vol. 7, no. 12, pp. 6842-6851, 2015/04/01 2015.

[19] S. Vallejos *et al.*, "Single-Step Deposition of Au- and Pt-Nanoparticle-Functionalized Tungsten Oxide Nanoneedles Synthesized Via Aerosol-Assisted CVD, and Used for Fabrication of Selective Gas Microsensor Arrays," *Advanced Functional Materials*, vol. 23, no. 10, pp. 1313-1322, 2013.

[20] M. Schweizer-Berberich *et al.*, "The effect of Pt and Pd surface doping on the response of nanocrystalline tin dioxide gas sensors to CO," *Sensors and Actuators B: Chemical*, vol. 31, no. 1, pp. 71-75, 1996/02/01/ 1996.

[21] K. Anand, J. Kaur, R. C. Singh, and R. Thangaraj, "Effect of terbium doping on structural, optical and gas sensing properties of In2O3 nanoparticles," *Materials Science in Semiconductor Processing*, vol. 39, pp. 476-483, 11// 2015.

[22] L. Chen, X. He, Y. Liang, Y. Sun, Z. Zhao, and J. Hu, "Synthesis and gas sensing properties of palladium-doped indium oxide microstructures for enhanced hydrogen detection," *Journal of Materials Science: Materials in Electronics*, vol. 27, no. 11, pp. 11331-11338, 2016.

[23] L. G. Bloor *et al.*, "Tantalum and Titanium doped In2O3 Thin Films by Aerosol-Assisted Chemical Vapor Deposition and their Gas Sensing Properties," *Chemistry of Materials*, vol. 24, no. 15, pp. 2864-2871, 2012/08/14 2012.

[24] S.-J. Choi *et al.*, "Selective Diagnosis of Diabetes Using Pt-Functionalized WO3 Hemitube Networks As a Sensing Layer of Acetone in Exhaled Breath," *Analytical Chemistry*, vol. 85, no. 3, pp. 1792-1796, 2013/02/05 2013.

[25] P. Van Tong, N. D. Hoa, N. Van Duy, D. T. T. Le, and N. Van Hieu, "Enhancement of gas-sensing characteristics of hydrothermally synthesized WO3 nanorods by surface decoration with Pd nanoparticles," *Sensors and Actuators B: Chemical*, vol. 223, pp. 453-460, 2016/02/01/ 2016.

[26] M. Ling and C. Blackman, "Growth mechanism of planar or nanorod structured tungsten oxide thin films deposited via aerosol assisted chemical vapour deposition (AACVD)," *physica status solidi (c)*, vol. 12, no. 7, pp. 869-877, 2015.

[27] S. Ashraf, C. S. Blackman, R. G. Palgrave, and I. P. Parkin, "Aerosol-assisted chemical vapour deposition of WO3 thin films using polyoxometallate precursors and their gas sensing properties," *Journal of Materials Chemistry*, 10.1039/B617982G vol. 17, no. 11, pp. 1063-1070, 2007.

[28] S. Vallejos *et al.*, "Au nanoparticle-functionalised WO3 nanoneedles and their application in high sensitivity gas sensor devices," *Chemical Communications*, 10.1039/C0CC02398A vol. 47, no. 1, pp. 565-567, 2011.

[29] M. Ling, S. Blackman Christopher, G. Palgrave Robert, C. Sotelo-Vazquez, A. Kafizas, and P. Parkin Ivan, "Correlation of Optical Properties, Electronic Structure, and Photocatalytic Activity in Nanostructured Tungsten Oxide," *Advanced Materials Interfaces*, vol. 4, no. 18, p. 1700064, 2017/09/01 2017.

[30] F. Y. Xie *et al.*, "XPS studies on surface reduction of tungsten oxide nanowire film by Ar+ bombardment," *Journal of Electron Spectroscopy and Related Phenomena*, vol. 185, no. 3, pp. 112-118, 2012/04/01/ 2012.

[31] J.-B. Lee, S.-Y. Jeong, W.-J. Moon, T.-Y. Seong, and H.-J. Ahn, "Preparation and characterization of electro-spun RuO2–Ag2O composite nanowires for electrochemical capacitors," *Journal of Alloys and Compounds*, vol. 509, no. 11, pp. 4336-4340, 2011/03/17/ 2011.

[32] F. E. Annanouch *et al.*, "Aerosol-Assisted CVD-Grown PdO Nanoparticle-Decorated Tungsten Oxide Nanoneedles Extremely Sensitive and Selective to Hydrogen," *ACS Applied Materials & Interfaces*, vol. 8, no. 16, pp. 10413-10421, 2016/04/27 2016.

[33] W. P. Sari, C. Blackman, Y. Zhu, and J. Covington, "Deposition of tungsten oxide and silver decorated tungsten oxide for use in oxygen gas sensing," in *2017 IEEE SENSORS*, 2017, pp. 1-3.

[34] K. Kanda and T. Maekawa, "Development of a WO3 thick-film-based sensor for the detection of VOC," *Sensors and Actuators B: Chemical*, vol. 108, no. 1, pp. 97-101, 2005/07/22/ 2005.

[35] S. Luo, G. Fu, H. Chen, and Y. Zhang, "Gas sensing properties and complex impedance analysis of La2O3-added WO3 nanoparticles to VOC gases," *Materials Chemistry and Physics*, vol. 109, no. 2, pp. 541-546, 2008/06/15/ 2008.

[36] S. Luo, G. Fu, H. Chen, Z. Liu, and Q. Hong, "Gas-sensing properties and complex impedance analysis of Ce-added WO3 nanoparticles to VOC gases," *Solid-State Electronics*, vol. 51, no. 6, pp. 913-919, 2007/06/01/ 2007.

[37] J. Fonollosa, L. Fernández, A. Gutiérrez-Gálvez, R. Huerta, and S. Marco, "Calibration transfer and drift counteraction in chemical sensor arrays using Direct Standardization," *Sensors and Actuators B: Chemical*, vol. 236, pp. 1044-1053, 2016/11/29/ 2016.

[38] R. Ionescu, E. Llobet, J. Brezmes, X. Vilanova, and X. Correig, "Dealing with humidity in the qualitative analysis of CO and NO2 using a WO3 sensor and dynamic signal processing," *Sensors and Actuators B: Chemical*, vol. 95, no. 1, pp. 177-182, 2003/10/15/ 2003.

[39] M. Hübner, C. E. Simion, A. Haensch, N. Barsan, and U. Weimar, "CO sensing mechanism with WO3 based gas sensors," *Sensors and Actuators B: Chemical*, vol. 151, no. 1, pp. 103-106, 2010/11/26/ 2010.

[40] V. Srivastava and K. Jain, "Highly sensitive NH3 sensor using Pt catalyzed silica coating over WO3 thick films," *Sensors and Actuators B: Chemical*, vol. 133, no. 1, pp. 46-52, 2008/07/28/ 2008.

[41] N. V. Hieu, V. V. Quang, N. D. Hoa, and D. Kim, "Preparing large-scale WO3 nanowire-like structure for high sensitivity NH3 gas sensor through a simple route," *Current Applied Physics*, vol. 11, no. 3, pp. 657-661, 2011/05/01/ 2011.

[42] N. Yamazoe, "New approaches for improving semiconductor gas sensors," *Sensors and Actuators B: Chemical*, vol. 5, no. 1, pp. 7-19, 1991/08/01/ 1991.

[43] C. Wang, L. Z. Yin, L., D. Xiang, and R. Gao, "Metal Oxide Gas Sensors: Sensitivity and Influencing Factors. Sensors " *Sensors*, vol. 10, no. 3, pp. 2088-2106, 2010.

[44] S. Rtimi, R. Sanjines, C. Pulgarin, A. Houas, J. C. Lavanchy, and J. Kiwi, "Coupling of narrow and wide band-gap semiconductors on uniform films active in bacterial disinfection under low intensity visible light: Implications of the interfacial charge transfer (IFCT)," *Journal of Hazardous Materials*, vol. 260, pp. 860-868, 2013/09/15/ 2013.

[45] D. P. Kumar, N. L. Reddy, M. Karthik, B. Neppolian, J. Madhavan, and M. V. Shankar, "Solar light sensitized p-Ag2O/n-TiO2 nanotubes heterojunction photocatalysts for enhanced hydrogen production in aqueous-glycerol solution," *Solar Energy Materials and Solar Cells*, vol. 154, pp. 78-87, 2016/09/01/ 2016.

[46] G. R. Bamwenda, K. Sayama, and H. Arakawa, "The effect of selected reaction parameters on the photoproduction of oxygen and hydrogen from a WO3–Fe2+–Fe3+ aqueous suspension," *Journal of Photochemistry and Photobiology A: Chemistry*, vol. 122, no. 3, pp. 175-183, 1999/03/31/ 1999.